

# Time-Resolved Thermoreflectance Imaging for Thermal Testing and Analysis

**Kazuaki Yazawa, Dustin Kendig**  
Microsanj LLC., Santa Clara, CA USA  
kaz@microsanj.com, +1-408-256-1255

**Ali Shakouri, Kazuaki Yazawa**  
Purdue University, West Lafayette, IN USA

## Abstract

High speed, time-resolved, thermoreflectance imaging is a novel way to locate defects or regions of potential failures in microelectronic devices. This paper reports on our thermoreflectance technique for dynamic imaging of circuit temperature distributions. This transient imaging method is based on a precise electrical lock-in technique with image processing similar to an old fashioned animation movie. An ordinal shutter speed camera is used in conjunction with an illumination LED that is pulsed for sampling the temperature distribution. This paper presents the method and gives a description of the system hardware. A theoretical comparison to lock-in thermography, which is based on infrared emission imaging, will be given. Limitations of thermoreflectance and the driving factors for spatial and time resolution will be discussed. Finally, we highlight and provide examples of near infrared (NIR) wavelength imaging, to enable both through-silicon thermal imaging and emission imaging in the same system. The combination of these two techniques is expected to enable hotspot temperatures and any anomalous emission sites to be correlated, hopefully leading to a better understanding of the nature of the defect.

## Introduction

Detecting a time-dependent defect and identifying it as a potential failure or gaining an understanding of the failure mechanisms related to the defect is a challenge in failure analysis for today's complex high-speed electronic devices. The scaling of device features results in a significant reduction in their time response and an increased sensitivity to transient events [1]. For example, a transient temperature change can result in a functional failure in a circuit with a tight design margin because of the timing perturbation caused by a small capacitance drift [2]. As device features shrink, the probability of detecting defects is also greatly reduced, thus leading to the development of statistics-based, large-area sampling methods [3]. Weaker signals and a lower probability of failure detection have made the understanding of the failures more difficult, but yet still very important.

Some failures and defects can only be effectively isolated with the aide of thermal information that is obtained while the semiconductor devices are operating, or, at a minimum, while a bias is applied to the defective circuit. A "short circuit" defect caused, for example, by a whisker, or by a very minor local misalignment of circuit features can produce highly concentrated Joule heating, even with a very small amount of dissipated power. While some detection methods have been developed for these cases, they are effective only under limited conditions [5]. One major problem is the rapid diffusion of heat, which blurs the hotspot and makes localization difficult using DC/static techniques.

Using a high speed transient imaging technique such as time-resolved thermoreflectance instead of static imaging enables weak heat signals to be captured and localized before the heat completely diffuses. This technique is capable of analyzing the small changes in temperature of the detailed features of a microelectronic device, while the device is driven under specific time-varying conditions such as a work load vector or a time varying bias.

Besides providing better localization capability, time-resolved thermoreflectance is also useful for analyzing the time-dependence of hotspot locations. By acquiring a time sequence of images in accordance with a time-varying workload, unexpected transient hotspot locations can be identified. These hotspots could be an indication of a logic failure, a timing failure, or a circuit design anomaly.

The thermoreflection concept itself has been known for some time, but its utilization for thermal analysis and defect detection has been limited. The current availability of turn-key systems, reduced complexity and cost, and innovations with CCD imaging and synchronization techniques has greatly enhanced the utility of this approach [4]. One recent innovation is the incorporation of photon emission imaging in a NIR thermoreflectance system. This combination enables comparisons to be made between hotspot and photon emission sites and makes it possible to analyze their correlations. Examples of backside imaging and the application of this combination will be shown. This paper will also provide the

theoretical background for thermoreflectance imaging and will describe its performance, capabilities, and limitations.

## 1. Thermoreflectance Imaging

### Physics of Thermoreflectance

Thermoreflectance is based on the change in surface reflectivity as a function of a material's temperature. Thermoreflectance with a pump-probe laser source has been widely used as a non-contact technique for measuring material thermal properties [6] [7]. The physical mechanism of this phenomenon is explained by the temperature dependence of a material's refractive index. On a microscopic view, the refractive index is temperature-dependent since the distance between atoms varies, and, hence, the material's bandgap varies, with temperature. This results in a slight change in reflectivity of the material.

The relationship between the change in reflectivity and the change in material temperature is usually expressed as a linear approximation when the temperature variation is small, e.g. 20 – 120 °C [8]. The amount that the reflectivity changes with temperature is called the thermoreflectance coefficient, which is a property of the reflective surface for the incident light wave. The thermoreflectance coefficient is found as,

$$\frac{\Delta R(\lambda)}{R(\lambda)} \approx \frac{1}{R(\lambda)} \frac{\partial R}{\partial T} \Delta T = C_{th}(\lambda) \Delta T \quad (1)$$

where  $R(\lambda)$  is the local reflection intensity,  $T$  is the local temperature, and  $C_{th}$  is the thermoreflectance coefficient.  $C_{th}$  is a material property that is only a function of the illumination wavelength,  $\lambda$ , for a homogeneous surface of a homogeneous material [4].

The thermoreflectance coefficient is quite dependent on wavelength [9]. It is non-zero for many materials over most of the visible wavelength range, but there are notable exceptions. For example, oxidized aluminum and oxidized silicon have a thermoreflectance coefficient near  $1 \times 10^{-4}$  for much of the visible wavelength range, but gold has a peak of approximately  $4 \times 10^{-4}$  at 470 nm (blue light), goes through zero at around 500 nm, and has a negative peak at about 530 nm [9].

### Hardware Setup and Operation

The thermal characterization setup is shown in Figs. 1 and 2.

#### 1) Imaging

A scientific grade, Si CCD camera with greater than 1 mega pixels is used for visible wavelengths. In combination with an optical microscope, the field of view (FOV) on the target device can be adjusted by the choice of objective lens. 1x to 100x magnification, air-gap objectives are available. For this setup, the camera pixel pitch is 12  $\mu\text{m}$  and the FOV is 2.46 mm x 2.46 mm with a 5x lens.

For near infrared (NIR) illumination in the range of 750-1400 nm, the Si CCD camera is replaced with a 640 x 512 pixel InGaAs camera. This camera has 25  $\mu\text{m}$  pixel pitch and 3.2 mm x 2.56 mm FOV with a 5x lens. Use of NIR wavelengths and an InGaAs sensor enables thru-substrate imaging for flip-chip applications. It also supports the use of illumination wavelengths beyond the visible to more fully exploit the wavelength dependence of thermoreflectance.

#### 2) Illumination and Wavelength

Because the thermoreflectance coefficient is wavelength dependent, the optimum LED illumination wavelength depends on the surface material being imaged. A wide range of visible and NIR wavelengths are available to select from. An optical bandpass filter, matched to the chosen wavelength, is placed in the detection path to eliminate background noise from ambient light, and thereby improve signal-to-noise ratio (SNR). The LED is electrically pulsed to provide short ( $\geq 100\text{ns}$ ) sampling pulses of light.

#### 3) Lock-in signals

Precise synchronization of the repetitive device bias signals, the LED pulses, and the camera is required for imaging the time dependent temperature response of the device. This synchronization is performed by the system's timebase electronics. Camera synchronization is achieved using an electronic imaging shutter. The timing delay of the LED illumination pulses relative to the device excitation is controlled for each camera exposure, as shown in Fig. 3. A time series of thermal images can be captured by continuously shifting this delay. To calibrate temperature automatically, the reflection intensity is measured at both the on and off portions of the device bias cycle, and the difference taken.

This technique directly captures thermal images in the time domain and has many advantages, including direct interpretation of the images and time resolution as low as 100 ns (and even lower with pulsed laser sources). Frequency-domain (FD) techniques can also be used to reveal useful information about the dynamic behavior of a device. These FD techniques have several advantages, including better noise rejection and sensitivity. As a result, they have a wide range of applications for different types of devices. However, FD techniques provide information in a more abstract form and have lower (worse) time resolution [10].

#### 4) NIR thermal imaging

As is well known, silicon is transparent for an illumination wavelength of around 1100 nm or longer, which is in the NIR range. This is convenient for thermal imaging of the device layer of a flip chip mounted device by viewing through the silicon substrate. Flip chip mounting is popular for today's high speed logic ICs. NIR thermoreflectance employs much of the same equipment and uses the same image data processing techniques. The main differences are in the optics (optimized for NIR transmission), imaging sensor (InGaAs versus Si), and LED (NIR instead of visible wavelength). In this setup, the current choices of illumination wavelengths are 1050, 1200,

1300, and 1500 nm. Depending on substrate doping and wavelength, imaging through full thickness Si substrates is possible.

5) *Photon emission imaging*

It is well known that detectable photon emission can be generated at electron ‘hotspots.’ In silicon, these are regions where current flows under high electric field conditions. To detect this emission, sensors with NIR wavelength sensitivity are required. Sensors with the ultimate sensitivity are typically fabricated from InGaAs or HgCdTe and cryogenically cooled to reduce the dark current for better SNR. Depending on the emission strength, non-cooled InGaAs cameras can also be used. Fortuitously, the useful wavelength range for photon emission overlaps the range for NIR thermoreflectance. Hence, the same setup can be used for imaging both thermal and electron hotspots.

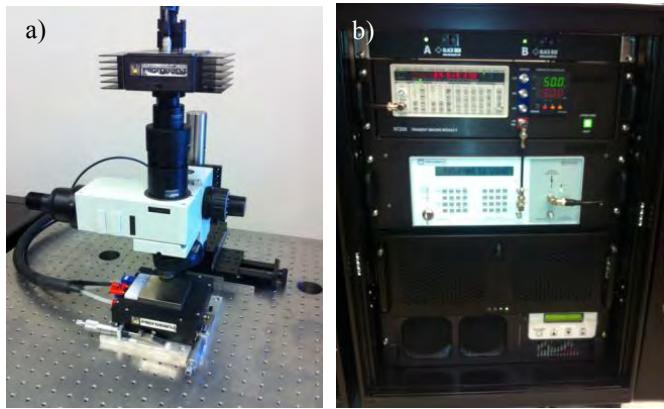


Figure 1: Picture of the system a) microscope setup and b) signal inter-lock and processing unit.

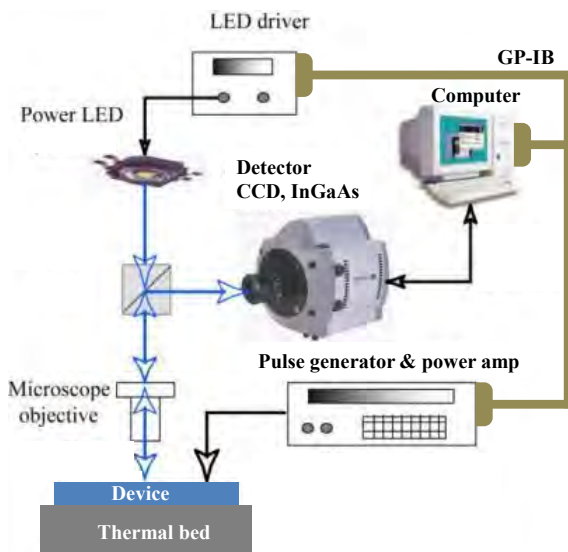


Figure 2: Schematic of the setup

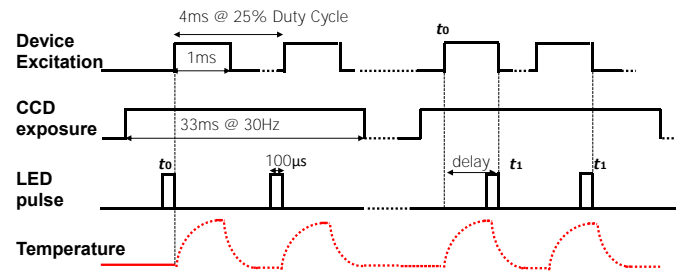


Figure 3: Timing diagram for an example of transient thermoreflectance measurement.

**Resolution and Sensitivity**

1) *Temperature*

Temperature resolution of the system is limited by photon shot noise because of the weak illumination from the short LED sampling pulses. This shot noise gives rise to random intensity fluctuations that is reduced through heavy averaging. The signal to noise ratio (SNR) of the measurement increases with the number of averages taken,  $n$ , as follows [11]:

$$SNR \propto \sqrt{n} \tag{2}$$

Temperature resolution of around 10-50 mK is achievable in practice. This is possible despite the 12-bit depth of the camera’s digitizer because noise dithers the signal across multiple bits and allows the heavily averaged signal to have an effective resolution of 18-bits [10]

Absolute temperature can be determined by referencing the thermoreflectance measurement against a direct measurement made, e.g., using a calibrated thermocouple. The thermocouple can be attached to an insensitive area of the device substrate to minimize its perturbation. It is not necessary to perform this calibration every time a measurement is made; however, calibration is dependent on the surface material and its finish, e.g., oxidized, plated, coated, level of surface roughness, etc. A more detailed calibration process is described in Ref [12].

2) *Spatial resolution*

At low magnification, the spatial resolution of the system is essentially given by the camera pixel pitch divided by the overall magnification of the optics. At higher magnifications, spatial resolution is limited by diffraction:

$$d = \frac{\lambda}{2(n \sin \theta)} \tag{3}$$

where  $d$  is the resolution,  $\lambda$  is the wavelength of the illuminating light source,  $\theta$  is a half angle from the light source over the entire optical system, and  $n$  is the index of refraction [13]. The product  $n \sin \theta$  is the numerical aperture,  $NA$ . From the above equation, spatial resolution can be increased ( $d$  decreased) by using shorter wavelengths and/or by increasing the numerical aperture. Standard air-gap objectives have an upper NA limit of 1, giving  $d \approx \lambda/2$ . For front-side devices (using visible wavelength light), the spatial resolution is  $d \approx 250\text{-}300\text{nm}$  for our system. For NIR imaging,

the spatial resolution limit of our setup is approximately 500 nm.

It is important to note that spatial resolution is a measure of how close two objects can be while still being distinguishable in an image. It does not place a lower limit on how well an isolated feature can be localized. It is also important to realize that regardless of the size of a defect, thermal propagation/spreading will result in the defect being imaged as a much larger object. Hence, thermoreflectance imaging provides the potential to precisely localize a hotspot which is physically 100 nm in size, for example, even though the diffraction limit is on the order of 250-300 nm.

### 3) Time resolution

Achieving the ultimate time resolution requires careful consideration of the high speed electrical signal transport required for the device biasing. An on-off pulsing cycle of 10 ns, for example, translates to a 100 MHz square wave. At this high pulse rate, the signal integrity of every part of the circuit must be carefully considered. A 50 ohm impedance match is required to avoid unwanted signal reflections since the high speed signal generation equipment is designed for 50 ohms. Additionally, the interaction of the optical on/off switching for the coherent light illumination needs to be carefully considered for high speed imaging. The details to enable 800 ps time resolution are reported in [14].

Time resolution is related to spatial resolution because heat diffusion is a function of time. If the temperature reading error due to this relationship is assumed to be 1% or less, the time resolution will be equal to or less than the following  $\Delta t$  [11]:

$$\Delta t = \frac{0.02}{\alpha} x^2 \quad (4)$$

where  $x$  is the length scale or resolution, in m, and  $\alpha$  is the thermal diffusivity of the material, in  $\text{m}^2/\text{s}$ . For example, a spatial resolution of 2  $\mu\text{m}$  requires approximately 1 ns time resolution for pure silicon, assuming 1% temperature error.

### 4) Thermal diffusion length and time delay

If an object is opaque, thermoreflectance can only measure its surface temperature. However, it is still possible to examine defects beneath opaque layers through the time response of the heating effect of the defect. If specific information about the materials and thicknesses of the intervening layers are available, the time delay between the applied bias pulse and when the thermal signal reaches the surface of the opaque layer(s) provides an indication of the depth of the defect. The depth of the defect location is calculated using the following equation:

$$\mu = 2\sqrt{\alpha t} \quad (5)$$

where  $t$  is the thermal time delay between the opaque surface and the defect location at depth  $\mu$  (which is the effective diffusion length) and  $\alpha$  is the effective thermal diffusivity of

the material in between. For copper, the effective diffusion length for a 100 ns time delay, is about 6.3  $\mu\text{m}$ .

### 5) Emission sensitivity

As stated earlier, the sensitivity in the 900 nm to slightly over 1500 nm wavelength range for the imaging sensor provides the capability to simultaneously characterize both emission distribution and thermal distribution through a silicon substrate. We investigated the sensitivity of the InGaAs uncooled camera in our setup with a device having a single known short circuit with its corresponding energy dissipation. We found the effective sensitivity of one pixel for emission to be about 30  $\mu\text{W}/\mu\text{m}^2$ .

## Comparison to Similar Technologies

### 1) Lock-in Thermography

Thermography is a common method for making non-contact temperature measurements. It uses cameras that are sensitive over the mid-wavelength infrared (MWIR) range (3000-8000 nm) to detect the black body radiation emitted by heated objects. InSb or HgCdTe sensors are typically used. They are normally cryogenically cooled to improve sensitivity.

The power radiated by a black body is given by the Stefan-Boltzmann law. The fourth order temperature dependence gives the technique its temperature sensitivity. For real materials, radiated power is also proportional to the material's emissivity. Every surface has a different emissivity, which depends on the angle over which the radiation is collected. Since the collection angle varies from the center to the edge of the field-of-view of the camera, calibration of the entire surface in the observed view must be done before accurate temperature maps can be made.

For transient measurements, conventional thermography is limited by the relatively slow time response (few ms) of the camera. Partially to work around this limitation, a lock-in technique was introduced for thermography that is similar to time-dependent thermoreflectance [15] [16] [17]. The working principle of lock-in thermography is similar to thermoreflectance and its setup is simpler since it does not require external illumination for the measurement. An external pulse generator provides signals to power the device and synchronize the image sensor. Even if transient analysis is not required, conventional thermography benefits from the lock-in technique because of its improved SNR through better noise rejection.

The typical time resolution for lock-in thermography is longer than 1  $\mu\text{s}$  [17], which is limited by the usable image data integration time of the camera: Similar to thermoreflectance, temperature resolution can be degraded by noise as time resolution is increased. This is a direct result of the required reduction in data integration time necessary for achieving higher time resolution.

### 2) Scanning Interferometry

Litzenberger, et al., reported the frequency domain phase shift detection technique for interferometry [18]. The phase shift information indirectly represents the thermal components. Since interferometry gives precise and microscopic information of thermal expansion, this approach could provide higher resolution and accuracy. Due to the optical modulation for detecting the phase shifts, the mechanical setup can be complex. A coherent illumination source, e.g. laser, is required.

### 3) Emission Microscopy

This technique is not for thermal analysis but can be used for detecting local circuit failures. Equipment specifically designed and optimized for emission microscopy (EMMI) can provide higher resolution and better SNR, but is significantly more expensive. The photon emission mechanism is typically one of the following: (1) electron-hole recombination, or (2) NIR photon emission by hot electron thermalization. The light generated by a defect may be very faint. Therefore, to passively detect the failure, the imaging sensor must have very high photon sensitivity in the wavelength range of interest. Typically, cooled InGaAs detectors are used.

## 2. Thermoreflectance examples

Local hotspots are indications of concentrated power dissipation that can arise from both defects, such as an electrical short, and from the normal operation of a device, such as the intentionally injected currents required for switching operations. In the following example, we demonstrate the high-resolution capability of this thermal technique by imaging and analyzing a small hotspot from the back side of a flip-chip mounted device.

Fig. 4 shows a through substrate thermoreflectance image of a hot-spot in a multi-finger MOSFET gate. The hot-spot is a simulated defect, induced by with an out of spec applied bias, in a 625  $\mu\text{m}$  thick silicon IC. The hotspot full-width-at-half-maximum (FWHM) size is measured to be 1.4  $\mu\text{m}$ , according to the line-scan shown in Fig. 5, taken across the hotspot. The overlay of the optical image and thermal image shows the precise location of the defect on the transistor. The averaging time for this particular case was 3 minutes and the temperature resolution was approximately 0.1  $^{\circ}\text{C}$ .

Since for this particular case, the hot spot is not due to standard in-spec operating conditions, the absolute temperature was not an important consideration. However, by knowing the surface material for the location or knowing the reflectance coefficient for the specific location, the absolute temperature can be automatically calculated by the system software.

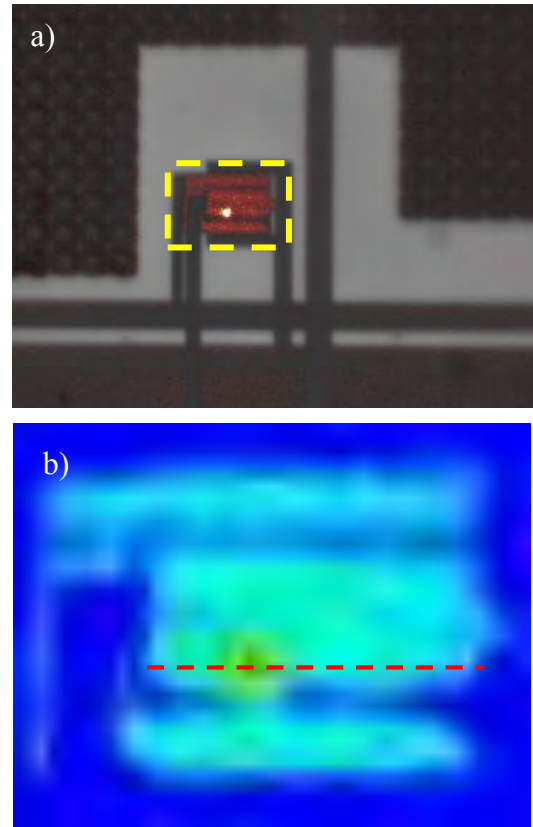


Figure 4. a) Thermal intensity over optical image with 50x zoom and b) temperature contour of the rectangular area of a MOSFET with an induced gate failure.

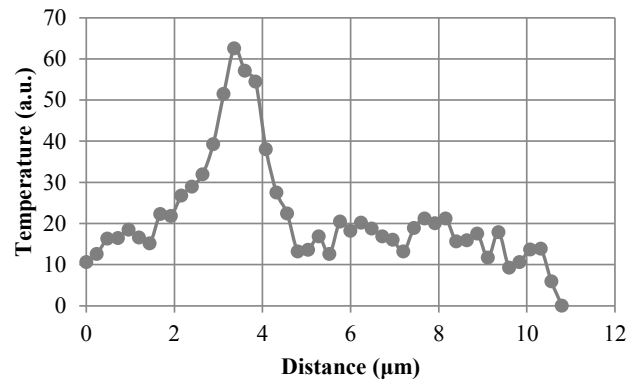


Figure 5. Temperature distribution along the line shown in Fig. 4b). The FWHM length of the hotspot is found to be 1.4  $\mu\text{m}$  by curve fitting.

The next example demonstrates the transient analysis capability of the system on a logic IC. The chip is 1.6 mm x 1.1 mm and 500  $\mu\text{m}$  thick, and is wire-bonded and decapsulated for thermal imaging from the front side. We evaluated the chip's thermal response as power was applied to it. Figure 6 shows the optical image of the tested chip while Fig. 7 shows a time series of the thermal intensity map, which is translated into a temperature map at the specified time after

power was applied. Figure 8 shows a 3D plot of temperature on the 2D surface, 3 ms after the device is powered on.

According to the time sequence shown in Fig. 7, the left side of the chip begins heating immediately after the application of power. After about 0.9 ms, another circuit starts dissipating power. From an analysis of the circuitry, the initial heating up of the left side was expected of a healthy device. The secondary heating after 0.9 ms was determined to be an unexpected latch-up failure, the location of which is indicated by the circle in Fig. 8.

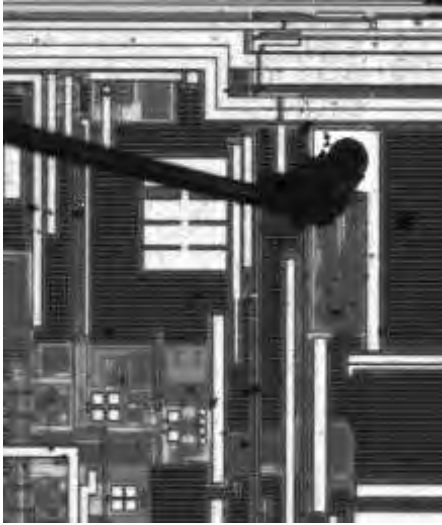


Figure 6. Optical 20x zoom image of the target circuit on a logic IC with 20x zoom.



Figure 7. Thermal response of the circuit.

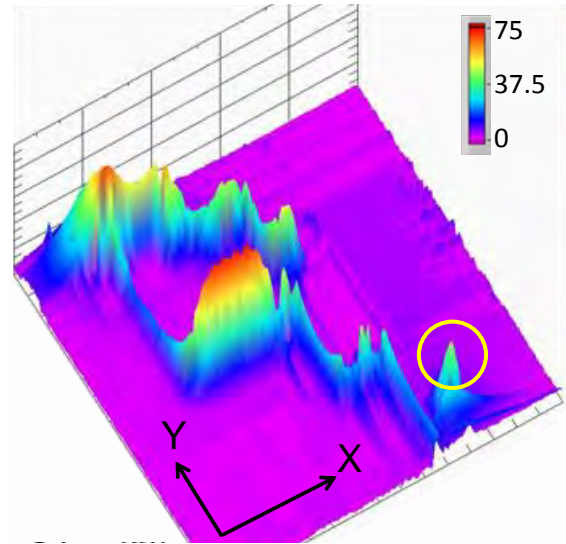


Figure 8. 3D plot of thermal profile on the area of interest in above figures. Vertical axis and color contour show the temperature excess in Kelvin and X axis and Y axis indicate the location on the target chip. The circle indicates the location of the latch-up.

Figure 9 shows an example of combined emission and thermal imaging through the silicon substrate. This figure shows the overlay of both signals on the optical image. Photon emission was detected by the uncooled InGaAs array sensor. The size of the emission spots are about  $5\ \mu\text{m} \times 2\ \mu\text{m}$ , as determined from the 50x zoom image. For this particular target device, we had the ability to directly drive the circuit and change the applied voltage. For the images shown,  $43.5\ \mu\text{W}$  of power was dissipated by the device where the emission signal was observed. It was the sensitivity limit for this case by using the sensor with 65% of quantum efficiency and its noise level is  $2.5 \times 10^9$  photons/cm<sup>2</sup>.s.

This example is provided for demonstration purposes only since this particular device did not have any known failures and also did not have a thermal issue. The two hotspots in the figure were induced by high current concentration of power lines and the temperature observed was at a normal level for the design. The emission signals are completely isolated from the thermal hotspots, as seen in the figure as well as in the circuitry. The locations of the emission sites were already known from EMMI for this particular device before our test. However, the thermal hot-spots were not detected prior to our test. With a stand-alone EMMI system or a stand-alone thermal detection system, detecting both sets of sites would have required two separate tests.

According to Arrhenius's law, many device failures can be predicted by the temperature at the location of interest. Leakage or short circuit defects may raise the temperature for the neighboring circuitry and could result in a shorter operating life, even if the leakage or short circuit defect does not interfere with circuit operation. Therefore, potential

reliability failures can be predicted if emission and thermal hot-spot locations were discovered in close proximity.

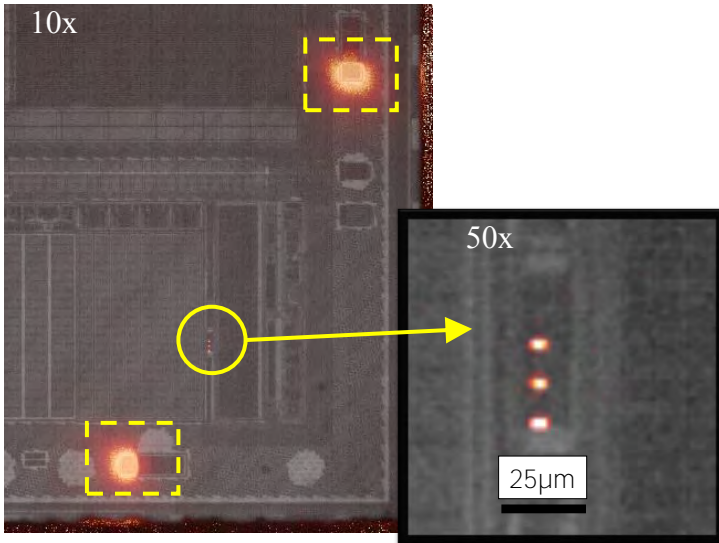


Figure 9. Overlay image of emission and thermal on an optical image, all acquired through the silicon substrate. Illumination is 1300 nm. Strong emission signal is observed in the encircled region, and thermal hotspots are found in the rectangular areas.

### 3. Detecting Footprint of Failures

The following early stage example illustrates the potential of time-resolved thermoreflectance for detecting and determining the depth of a defect beneath an optically opaque interface, such as a metal layer. This technique depends on measuring the time delay of the thermal signal and then calculating the thermal diffusion length if the knowledge of the precise structure, dimensions, and material properties of the intervening layers given. As discussed earlier, the calculated thermal diffusion length is the estimated depth of the defect below the opaque interface.

For this particular test case, shown schematically in Fig 10a, the first layer we were able to observe through the silicon substrate was made of poly resistor material. The known defect was located deep under 6 layers of copper traces. Hence, the target hotspot was invisible and impossible to directly reach with any light wavelength we could use. However, by imaging the topmost layer using the time-resolved thermoreflectance method (Figs. 10b and 10c) the thermal propagation delay of the hotspot through the layers could be determined (Fig. 11).

The hotspot visible in Fig. 10c (red spot, arrow) is the thermal signal that is produced by the buried defect, as it appears at the topmost metal layer. The traces shown in Fig. 11 are the time-resolved temperature profiles measured at a poly resistor on the top metal layer (blue, triangles) and at the hotspot location shown in Fig. 10c (red, squares). The time response delay was

observed approximately 75  $\mu$ s. This value seems very large with assuming the copper layers. The delay time is likely dominated by oxide layers or passivation layers separating metal layers, which have nearly  $10^4$  times smaller thermal diffusivity, e.g.  $0.83 \times 10^{-8}$   $m^2/s$  for  $SiO_2$ , compare to  $1.1 \times 10^{-4}$   $m^2/s$  for copper. Based on the knowledge of the hotspot location, this observed thermal propagation must be due to the arrival of thermal propagation to the topmost layer from the buried hotspot with this time delay.

In this particular test case, the defect location in the chip was provided. We demonstrated the ability to observe the heat propagation to the top metal layer at the location of the known short circuit defect. In an actual FA situation, the actual hotspot depth would, of course, be unknown. To utilize this method for such blind work, we will need more examples to confirm this capability to quantize the cause-and-effect relations. It remains a work in progress.

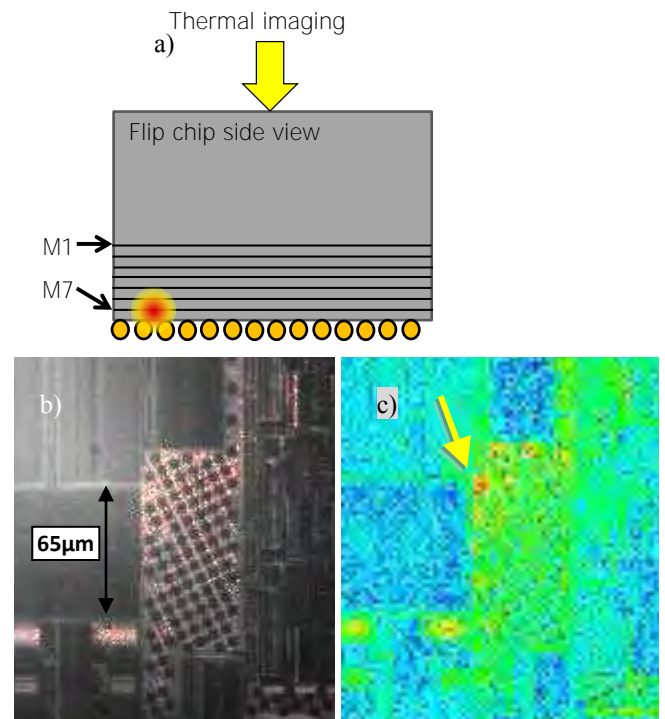


Figure 10. Detection of a short circuit failure underneath 6 metal layers, taken through the silicon substrate. The back side thermal image was taken with 1050 nm LED and 50x objective. a) shows the structure of the device (side view), b) shows the thermal signals overlaid on an optical image, and c) shows the thermal contour, blue is cold and red is hot.

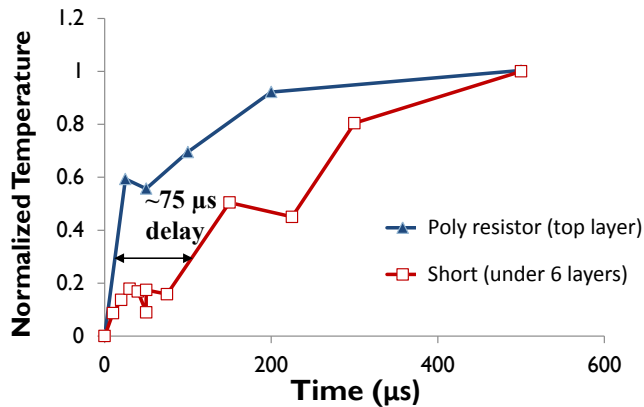


Figure 11. Normalized temperature response at the top metal layer (M1). The time delay from the heating on top and heating from the short circuit is observed.

### Conclusions

High speed time-resolved thermoreflectance imaging is introduced with its physical background. Due to the wide selection of illumination wavelengths, this interlocking thermoreflectance imaging method provides through silicon substrate thermal imaging under specific workloads for the target device. A NIR sensitive camera is used for both thermoreflectance and emission imaging. The location, intensity, and time dependent profile of thermal hotspots and photon emission are captured in a single setup. Comparisons to (MWIR) lock-in thermography and emission microscopy were also provided. Discussions included the limitations of the various techniques and the driving factors for their spatial and time resolution.

A hotspot in a MOSFET caused by a gate failure was observed through a silicon substrate without any treatment (thinning or wrapping) on the back side. With 1300 nm illumination wavelength, the size of the hot spot was determined to be 1.4 μm. A simultaneous combination of high speed transient thermal imaging and emission imaging was shown on a logic device, through the substrate. In this particular example, unfortunately, the interaction between the emission and thermal hotspots was not observed. For cases in which both locations are in close proximity, potential reliability issues may be predictable:

The last example illustrates the potential for detecting a failure located below an opaque interface. The time delay information of the thermal propagation through the layers is captured by this time-resolved thermoreflectance method. In principle, with this information, and with knowledge of the thermal diffusion characteristics of the intervening material, the depth of the failure can be located. A full demonstration of this technique will be reported in the future.

### Acknowledgement

Authors acknowledge Dr. Joanna Kiljan and Qualcomm Inc. for generously providing the example devices with known failures for testing the capability of our thermoreflectance imaging system.

### References

- [1] Schaller, R.R., "Moore's law: past, present and future", *IEEE Spectrum*, Vol. 34 (6), 1997, pp.52-59.
- [2] Lefurgy, C.R., Drake, A.J., Floyd, M. S., Allen-Ware, M. S., Brock, B., Tierno, J.A., and Carter, J.B., "Active Management of Timing Guardband to Save Energy in POWER7", *Proc. 44th IEEE/ACM Int'l Symp. on Microarchitecture*, 2011, pp. 1-11
- [3] Riley, S.L., "Optical inspection of wafers using large-area defect detection and sampling", *Proc. IEEE Int'l Workshop VLSI Systems*, 1992, pp. 12 - 21
- [4] Farzaneh, M., Maize, K., Luerßen, D., Summers, J. A., Mayer, P. M., Raad, P. E., Pipe, K. P., Shakouri, A., Ram, R. J., Hudgings, J. A., "CCD-based thermoreflectance microscopy: principles and applications", *J. Phys. D: Appl. Phys.*, 42, 2009, 143001 (20pages).
- [5] Madian, A.H., Amer, H.H., Eldesouk, A.O., "Catastrophic Short and Open Fault Detection in MOS Current Mode Circuits: A Case Study", *Proc. 12<sup>th</sup> Biennial Baltic Electronics Conf.*, 2010, pp. 145-148.
- [6] Cahill, D.G., "Analysis of heat flow in layered structures for time-domain thermoreflectance", *Rev. Sci. Instrum.*, Vol. 75, 12, 2004, 5119 (4 pages) .
- [7] Taketoshi, N., Baba, T. and Ono, A., "Development of a thermal diffusivity measurement system for metal thin films using a picosecond thermoreflectance technique", *Meas. Sci. and Techn.*, Vol. 12 No. 12, 2001, pp. 2064-2073.
- [8] Tessier, G., Pavageau, S., Filloy, C., Charlot, B., Jerosolimski, G., Fournier, D., Cretin, B., Dilhaire, S., Gomes, S., Trannoy, N., Vairac, P., and Volz, S., "Quantitative Thermoreflectance Imaging Calibration Method and Validation on a Dedicated Integrated Circuit", *Proc. THERMINIC*, 2005.
- [9] Yazawa, K., Kendig, D., Raad, P. E., Komarov, P. L., Shakouri, A., "Understanding the Thermoreflectance Coefficient for High Resolution Thermal Imaging of Microelectronic Devices", *Technical Brief, Electronics Cooling Magazine*, March 2013, pp. 10-14.
- [10] Vermeersch, B., Christofferson, J., Maize, K., Shakouri, A., De Mey, G., "Time and Frequency Domain CCD-Based Thermoreflectance Techniques for High-Resolution Transient Thermal Imaging", *Proc. IEEE 26<sup>th</sup> SEMI-THERM*, 2010, pp. 228-234.
- [11] Yazawa, K., Kendig, D., Hernandez, D., Maize, K., Alavi, S., and Shakouri, A., "High Speed Transient Thermoreflectance Imaging of Microelectronic Devices and Circuits", *EDFA Magazine*, Vol. 15, 2013, pp. 12-22.

- [12] Microsanj LLC., Application Note, MS-AN-002, "Preparing Device Samples for Thermal Analysis and Thermal Mapping Using the Thermoreflectance Imaging Analyzer", [http://www.microsanj.com/sites/default/files/MSAN-002\\_Sample\\_Preparation\\_for\\_Thermoreflectance\\_Imaging\\_July\\_2012..pdf](http://www.microsanj.com/sites/default/files/MSAN-002_Sample_Preparation_for_Thermoreflectance_Imaging_July_2012..pdf)
- [13] Lipson, S.G., Lipson, H., and Tannhauser, D.S., Optical Physics Third Edition, Cambridge University Press (London, 1995), pp. 340.
- [14] Christofferson, J., Yazawa, K., Shakouri A., "Picosecond transient thermal imaging using a CCD based thermoreflectance system", *Proc. 14th Int'l Heat Transfer Conference*, 2010.
- [15] Breitenstein, O., Warta, W., Langenkamp, M., Lock-in thermography – Basics and Use for Evaluating Electronic Devices and Materials Second Ed., Springer, 2010.
- [16] Hefner, A., Berning, D., Blackburn, D., Chpuy, and C., Bouche, S., "A High-speed Thermal Imaging System for Semiconductor Device Analysis", *Proc. 17<sup>th</sup> IEEE SEMI-THERM Symp.*, 2001, pp. 43-49.
- [17] Pradere, C., Clerjaud, L., Batsale, J. C., and Dilhaire, S., "High speed heterodyne infrared thermography applied to thermal diffusivity identification", *Rev. Sci. Instr.* vol. 82, 2011, 054901.
- [18] Litzemberger, M., Fürböck, C., Bychikhin, S., Pogany, D., and Gornik, E., "Scanning Heterodyne Interferometer Setup for the Time-Resolved Thermal and Free-Carrier Mapping in Semiconductor Devices", *IEEE Trans. Instr. and Meas.*, Vol. 54, (6), 2005, pp. 2438-2445.